The effect of time-dependent creep on electro-thermo-mechanical behaviors of piezoelectric sphere using Mendelson's method

A. Ghorbanpour Arani, R. Kolahchi*, A.A. Mosallaie Barzoki, A. Loghman

Faculty of Mechanical Engineering, University of Kashan, Ghotbe Ravandi Boulevard, Kashan, Islamic Republic of Iran

ABSTRACT

This paper describes a numerical model which is used for the computation of stresses, electric potential and displacement histories in a hollow piezoelectric sphere subjected to an internal pressure and a distributed temperature field. The mentioned model is on the basis of the Mendelson's method which predicts the variation of the stresses, electric potential and displacement with time through the thickness. The creep constitutive model for the effective strain is on the basis of the Bailey–Norton's law. Since, creep strains are time, temperature and stress dependent, the closed form solution cannot be represented for this constitutive differential equation. Therefore, a semi-analytical method in conjunction with the method of successive approximation has been proposed for this analysis. The results indicate that in mechanical boundary condition which the sphere acts as an actuator, the effect of time-dependent creep causes to change radial stresses from compressive to tensile after 15 years. Hence, the actuator is not usable after 15 years. It has been found that in electrical boundary condition which the sphere acts as a sensor, the radial stresses are compressive during the life of the sphere. This state is suitable, because the sensor can be used for long time.

© 2012 Elsevier Masson SAS. All rights reserved.

1. Introduction

Piezoelectricity refers to an electromechanical phenomenon in particular solid state materials that demonstrates a coupling between their electrical, mechanical, and thermal states generated by applying mechanical stress to dielectric crystals. The direct piezoelectric effect describes the electrostatic reaction to a mechanical load such as sensors, while the converse piezoelectric effect describes the mechanical reaction to an electrostatic load such as actuators. Recently, application of piezoelectric materials in smart structures has been the subject of intense research. Devices based on piezoelectric elements are commonly used in industry and laboratories.

Although elastic analysis of hollow structures under electrical, thermal and mechanical loads are well developed (Dai and Wang, 2005; Ghorbanpour Arani et al., 2006; Dai and Fu, 2006; Babaei and Chen, 2008; Khoshgoftar et al., 2009; Ghorbanpour Arani et al., 2010; Wang and Xu, 2010; Ghorbanpour Arani et al., 2011) but a few publications for time-dependent creep behavior of spheres and cylinders can be found in the literatures. Loghman

and Wahab (1996) investigated creep damage simulation of thick-walled tubes using the theta projection concept. Yang (2000) presented a solution for time-dependent creep behavior of functionally graded material (FGM) cylinders using Norton's law for material creep constitutive model. Chen et al. (2006) analyzed creep deformation of a functionally graded cylinder subjected to internal and external pressures. You et al. (2007) considered steady state creep deformation and stresses in thick-walled cylindrical vessels of FGM subjected to internal pressure. Loghman and Shokouhi (2009) evaluated creep damages of thick-walled spheres using a long-term creep constitutive model. Time-dependent deformation and fracture of multi-material systems at high temperature were presented by Xuan et al. (2009). Tejeet and Gupta (2011) investigated effect of anisotropy on steady state creep in functionally graded cylinder. Magnetothermoelastic creep analysis of functionally graded cylinder was presented by Loghman et al. (2010). Later, time-dependent creep stress redistribution analysis of thick-walled spheres made of FGM subjected to an internal pressure and a uniform temperature field was performed by Loghman et al. (2011a) using the method of successive elastic solution. In another work, time-dependent creep stress redistribution analysis of rotating disk made of Al–SiC composite was investigated by Loghman et al. (2011b) using Mendelson's method of successive elastic solution. Hamed (2012) investigated the viscoelastic creep

response of flexural beams and beam-columns made with FGMs. This paper highlights the challenges associated with the modeling and analysis of such structures, and presents a nonlinear theoretical model for their bending and creep buckling analysis. A generalized constitutive model for describing the creep deformation and creep damage development in initially isotropic materials with characteristics dependent on the kind of the stress state was implemented by Zolochevsky et al. (2012) into the finite element analysis. Spathis and Kontou (2012) analyzed a theoretical approach for the prediction of creep rupture time of polymers and polymer composites. Loghman et al. (2012) studied magnetothermoelastic creep behavior of thick-walled spheres made of FGM placed in uniform magnetic and distributed temperature fields and subjected to an internal pressure using method of successive elastic solution. The elastic and elastic–plastic creep behavior of cracked structures in the presence of residual stress was studied numerically by Yazdani and O'Dowd (2012). None of the above research studies did consider electric loading due to piezoelectric material. A part from a couple of studies, prepared by a few authors here, little or no reference has been made so far in the literature on the time-dependent creep analysis of sphere.

However, in the present study, for the first time, time-dependent creep response of a hollow sphere made of radially polarized transversely isotropic piezoelectric material, such as BaTiO$_3$ is investigated using Mendelson's method of successive elastic solution. This paper aims to show the significant effect of time-dependent creep on stresses, electric potential and displacement histories during the life of a smart sphere.

2. Geometry, loading condition, material properties and creep constitutive model

2.1. Geometry and loading condition

A hollow sphere with constant thickness h, inner radius a, outer radius b and radius ratio of $a/b = 2$ is considered. The sphere is subjected to an internal and external pressure (P_a, P_b), a constant potential difference between its inner and outer surfaces and distributed temperature field due to steady state heat conduction from inner surface to outer surface of the sphere with inner temperature of $T_a = 323$ K and outer temperature of $T_b = 298$ K (Fig. 1).
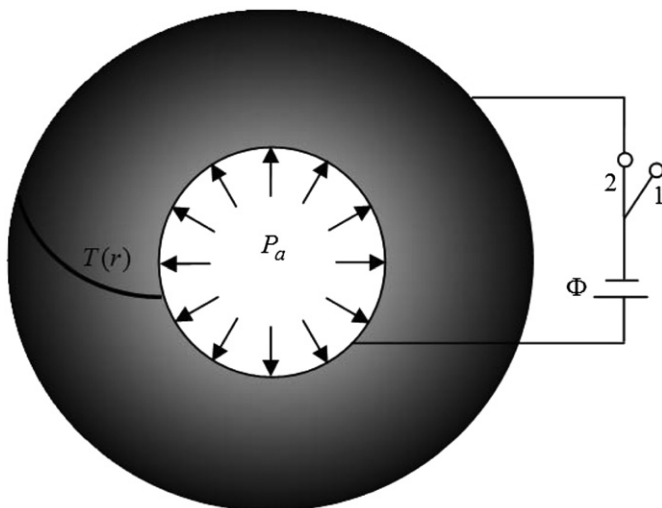

Fig. 1. Configuration of a hollow sphere in two states; 1 – actuator, 2 – sensor (without internal pressure).

2.2. Material properties

Ferroelectric materials are key to many modern technologies, in particular piezoelectric actuators and electro-optic modulators. BaTiO$_3$ is one of the most extensively studied ferroelectric materials. The use of BaTiO$_3$ for piezoelectric applications is, however, limited due to the small piezoelectric coefficient of the room temperature-stable tetragonal phase. It has been shown by Zhou and Kamlah (2006) that even at room temperature, ferroelectric piezoceramics exhibit significant creep effects. Therefore, in this study, BaTiO$_3$ is elected for the sphere. In the numerical calculations, the mechanical, electrical and thermal properties are taken as (Saadatfar and Razavi, 2009):

$$
\begin{aligned}
&C_{11} = 128\,(\text{GPa}), \quad e_{11} = 8.5\,(\text{C/m}^2), \quad\quad \alpha_r = 2 \times 10^{-6}\,(1/\text{K}),\\
&C_{22} = 150\,(\text{GPa}), \quad e_{12} = 1.61\,(\text{C/m}^2), \quad \alpha_\theta = 1 \times 10^{-6}\,(1/\text{K}),\\
&C_{23} = 37.1\,(\text{GPa}), \quad \in_{11} = 4.98 \times 10^{-9}\,(\text{F/m}),\\
&C_{12} = 32.3\,(\text{GPa}),
\end{aligned}
\tag{1}
$$

where $c_{ij}(i, j = 1, 2)$, $e_{1i}(i = 1, 2)$, $\alpha_i(i = r, \theta)$ and $\in_{11}$ are elastic, piezoelectric, thermal expansion and dielectric constants, respectively.

2.3. Creep constitutive model

In the present work, the material creep behavior is described by Bailey–Norton's constitutive model as follows (Penny and Marriott, 1995):

$$
\dot{\varepsilon}_e = Bt^n\sigma_e^m,
\tag{2}
$$

where B and m are the Norton's coefficients and n is the Bailey coefficient which can be defined as follows (You et al., 2007):

$$
B = 0.11 \times 10^{-21}, \quad m = 5, \quad 0.33 < n < 0.50
\tag{3}
$$

3. The constitutive equations for piezoelectric materials

A deformation in piezoelectric material generates an electric displacement at its surface, which is proportional to the strain applied and the surrounding electric field. On the other hand, an electric field applied to the piezoelectric material causes a strain, which is proportional to the field strength and additional stress applied to it, such as, e.g. a pre-load. The constitutive equations for a homogenous piezoelectric material can be written as (Jalili, 2010):

$$
\boldsymbol{\sigma} = \mathbf{C} : \boldsymbol{\varepsilon} - \mathbf{e} : \mathbf{E},
\tag{4}
$$

$$
\mathbf{D} = \mathbf{e} : \boldsymbol{\varepsilon} + \in : \mathbf{E},
\tag{5}
$$

where $\boldsymbol{\varepsilon}$, $\boldsymbol{\sigma}$, $\mathbf{E}$ and $\mathbf{D}$ are strain, stress, electric field and electric displacement tensors respectively. Also, $\mathbf{C}$, $\mathbf{e}$ and $\in$ are the fourth-order elasticity tensor, the third order tensor of piezoelectric coefficient and the dielectric permittivity tensor.

4. Formulation of the problem

In this study, it is assumed that, only the radial displacement (U_r) is nonzero and electric potential is the function of radial coordinate (r).

4.1. Derivation of equations

The equilibrium equation of the piezoelectric sphere in the absence of body force and the Maxwell's equation for free electric charge density are (Fungn, 1965; Tiersten, 1969):

$$\frac{d\sigma_{rr}}{dr} + \frac{2(\sigma_{rr} - \sigma_{\theta\theta})}{r} = 0, \tag{6}$$

$$\frac{\partial D_{rr}}{\partial r} + \frac{2}{r}D_{rr} = 0, \tag{7}$$

where $\sigma_{ii}(i = r, \theta)$ is the stress tensor and D_{rr} is the radial electric displacement.

Also, the radial and circumferential strains and the relation between electric field (E_{rr}) and electric potential (ϕ) are reduced to

$$\varepsilon_{rr} = \frac{\partial u}{\partial r}, \tag{8}$$

$$\varepsilon_{\theta\theta} = \varepsilon_{\zeta\zeta} = \frac{u}{r}, \tag{9}$$

$$E_{rr} = -\frac{\partial \phi}{\partial r}. \tag{10}$$

The constitutive relations of radially polarized piezoelectric sphere and the components of radial electric displacement vector can be written as (Salehi-Khojin and Jalili, 2008; Mendelson, 1968):

$$\left\{ \begin{matrix} \sigma_{rr} \\ \sigma_{\theta\theta} \end{matrix} \right\} = \begin{bmatrix} C_{11} & C_{12} & C_{13} \\ C_{21} & C_{22} & C_{23} \end{bmatrix} \left(\left\{ \begin{matrix} \varepsilon_{rr} \\ \varepsilon_{\theta\theta} \\ \varepsilon_{\theta\theta} \end{matrix} \right\} - \left\{ \begin{matrix} \alpha_r \\ \alpha_\theta \\ \alpha_\theta \end{matrix} \right\} T(r) - \left\{ \begin{matrix} \varepsilon_{rr}^c \\ \varepsilon_{\theta\theta}^c \\ \varepsilon_{\theta\theta}^c \end{matrix} \right\} \right)$$
$$- \begin{bmatrix} e_{11} \\ e_{12} \end{bmatrix} \{E_{rr}\} \tag{11}$$

$$\{D_{rr}\} = [e_{11} \quad e_{12} \quad e_{13}] \left(\left\{ \begin{matrix} \varepsilon_{rr} \\ \varepsilon_{\theta\theta} \\ \varepsilon_{\theta\theta} \end{matrix} \right\} - \left\{ \begin{matrix} \alpha_r \\ \alpha_\theta \\ \alpha_\theta \end{matrix} \right\} T(r) - \left\{ \begin{matrix} \varepsilon_{rr}^c \\ \varepsilon_{\theta\theta}^c \\ \varepsilon_{\theta\theta}^c \end{matrix} \right\} \right)$$
$$+ [\in_{11}]\{E_{rr}\}. \tag{12}$$

Considering transverse isotropic behavior of piezoelectric material, the elasticity and the piezoelectric tensors are summarized to

$$\begin{aligned} C_{12} &= C_{13} = C_{21}, \\ e_{12} &= e_{13}. \end{aligned} \tag{13}$$

4.2. Heat conduction problem

In this study, a distributed temperature field due to steady-state heat conduction has been considered. The heat conduction equation without any heat source is written in spherical coordinate as (Khoshgoftar et al., 2009; Jabbaria et al., 2002):

$$\frac{1}{r^2}\frac{\partial}{\partial r}\left(K_0 r^2 T'(r)\right) = 0, \tag{14}$$

$$\begin{aligned} \text{at } r = a \quad & T(r) = T_a, \\ \text{at } r = b \quad & \frac{\partial T(r)}{\partial r} + hT(r) = 0, \end{aligned} \tag{15}$$

where h is the ratio of the convective heat-transfer coefficient and K_0 is the nominal heat conductivity coefficient. Integrating twice Eq. (14) yields:

$$T(r) = \frac{-B_1}{r} + B_2, \tag{16}$$

where B_1 and B_2 are constants which can be obtained using thermal boundary conditions (Eq. (15)).

4.3. Dimensionless form of equations

It is appropriate to introduce the following dimensionless quantities as follows:

$$\sigma_i = \frac{\sigma_{ii}}{C_{22}}(i = r, \theta), \quad c_i = \frac{C_{1i}}{C_{22}}(i = 1, 2, 3), \quad E_i = \frac{e_{1i}}{E_0}(i = 1, 2, 3),$$

$$E_0 = \sqrt{C_{22}\in_{11}},$$

$$U = \frac{u_r}{a}, \quad \xi = \frac{r}{a}, \quad \eta = \frac{b}{a}, \quad \beta = \frac{\beta_1}{E_0}, \quad \Phi = \frac{\phi}{\phi_0}, \quad \phi_0 = a\sqrt{\frac{C_{22}}{\in_{11}}},$$

$$D_r = \frac{D_{rr}}{E_0}. \tag{17}$$

Using the above dimensionless variables, Eqs. (6), (7), (11) and (12) can be expressed as:

$$\frac{\partial \sigma_r}{\partial \xi} + \frac{2(\sigma_r - \sigma_\theta)}{\xi} = 0, \tag{18}$$

$$\frac{\partial D_r}{\partial \xi} + \frac{2D_r}{\xi} = 0. \tag{19}$$

$$\left\{ \begin{matrix} \sigma_r \\ \sigma_\theta \end{matrix} \right\} = \left(\begin{bmatrix} C_1 & C_2 & C_2 \\ C_2 & 1 & C_3 \end{bmatrix} \left(\left\{ \begin{matrix} \frac{\partial U}{\partial \xi} \\ \frac{U}{\xi} \\ \frac{U}{\xi} \end{matrix} \right\} - \left\{ \begin{matrix} \alpha_r \\ \alpha_\theta \\ \alpha_\theta \end{matrix} \right\} T(\xi) - \left\{ \begin{matrix} \varepsilon_{rr}^c \\ \varepsilon_{\theta\theta}^c \\ \varepsilon_{\theta\theta}^c \end{matrix} \right\} \right) \right.$$
$$\left. + \begin{bmatrix} E_1 \\ E_2 \end{bmatrix} \left\{ \frac{\partial \Phi}{\partial \xi} \right\} \right), \tag{20}$$

$$\{D_r\} = \left([E_1 \quad E_2 \quad E_2] \left(\left\{ \begin{matrix} \frac{\partial U}{\partial \xi} \\ \frac{U}{\xi} \\ \frac{U}{\xi} \end{matrix} \right\} - \left\{ \begin{matrix} \alpha_r \\ \alpha_\theta \\ \alpha_\theta \end{matrix} \right\} T(\xi) - \left\{ \begin{matrix} \varepsilon_{rr}^c \\ \varepsilon_{\theta\theta}^c \\ \varepsilon_{\theta\theta}^c \end{matrix} \right\} \right) \right.$$
$$\left. - \left\{ \frac{\partial \Phi}{\partial \xi} \right\} \right). \tag{21}$$

5. Solution of the problem

The solution of Eq. (19) is:

$$D_r = \frac{A_1}{\xi^2},\tag{22}$$

where A_1 is a constant. Substituting Eq. (22) into Eq. (21) and combination with Eq. (20), results

$$
\begin{aligned}
\left\{ \begin{matrix} \sigma_r \\ \sigma_\theta \end{matrix} \right\} = &\left(\begin{bmatrix} C_1 & C_2 & C_2 \\ C_2 & 1 & C_3 \end{bmatrix} \left(\left\{ \begin{matrix} \dfrac{\partial U}{\partial \xi} \\ \dfrac{U}{\xi} \\ \dfrac{U}{\xi} \end{matrix} \right\} - \left\{ \begin{matrix} \alpha_r \\ \alpha_\theta \\ \alpha_\theta \end{matrix} \right\} T(\xi) - \left\{ \begin{matrix} \varepsilon_{rr}^c \\ \varepsilon_{\theta\theta}^c \\ \varepsilon_{\theta\theta}^c \end{matrix} \right\} \right) \right. \\
&+ \begin{bmatrix} E_1 \\ E_2 \end{bmatrix} \left[E_1 \ \ E_2 \ \ E_2 \right] \left(\left\{ \begin{matrix} \dfrac{\partial U}{\partial \xi} \\ \dfrac{U}{\xi} \\ \dfrac{U}{\xi} \end{matrix} \right\} - \left\{ \begin{matrix} \alpha_r \\ \alpha_\theta \\ \alpha_\theta \end{matrix} \right\} T(\xi) - \left\{ \begin{matrix} \varepsilon_{rr}^c \\ \varepsilon_{\theta\theta}^c \\ \varepsilon_{\theta\theta}^c \end{matrix} \right\} \right) \\
&\left. - A_1 \xi^{-2} \right).
\end{aligned}
\tag{23}
$$

where $T(\xi)$ is temperature distribution which is illustrated in Eq. (16).

Finally, substituting Eq. (23) into Eq. (18) yields the following differential equation

$$
\begin{aligned}
\xi^2 \frac{\partial^2 U}{\partial \xi^2} + D_1 \xi \frac{\partial U}{\partial \xi} + D_2 U = &\, D_3 A_1 \xi^{-1} + D_4 B_1 \\
&+ \left(D_5 B_2 + D_6 \varepsilon_r^c + D_7 \varepsilon_\theta^c \right) \xi \\
&+ \left(D_8 \frac{\partial \varepsilon_\theta^c}{\partial \xi} + \frac{\partial \varepsilon_r^c}{\partial \xi} \right) \xi^2,
\end{aligned}
\tag{24}
$$

where $D_i (i = 1, \ldots 8)$ are defined in Appendix A.

5.1. Electro-thermo-elastic analysis of sphere

A semi-analytical method has been employed for solution of this differential equation (i.e. Eq. (24)). In this method, the solution domain is divided into some finite divisions as shown in Fig. 2. The coefficients of Eq. (24) are evaluated at ξ^m, mean radius of mth division, and therefore, differential equation with constant coefficients becomes valid only in mth sub-domain which can be rewritten as follows (Kordkheili and Naghdabadi, 2007; Bayat et al., 2009)

$$\left(M_1^m \frac{d^2}{dr^2} + M_2^m \frac{d}{dr} + M_3^m \right) U^m + M_4^m = 0,\tag{25}$$

$$M_1^m = (\xi^m)^2,\tag{26}$$
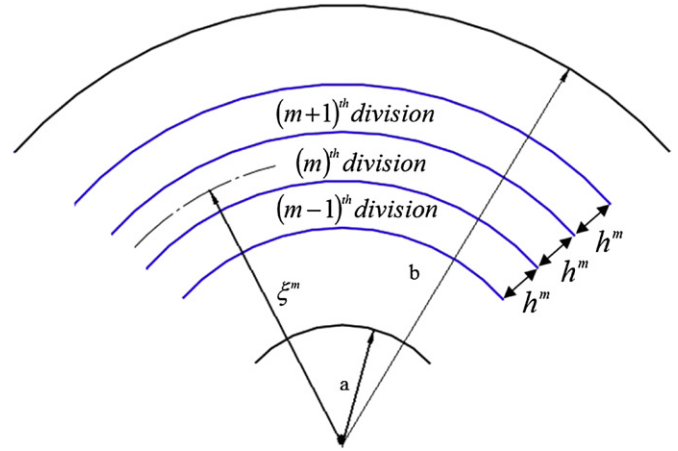
$$M_2^m = D_1 \xi^m,\tag{27}$$

$$M_3^m = D_2,\tag{28}$$

Fig. 2. Illustration of some finite sub-domains in radial domain.

$$
\begin{aligned}
M_4^m = &\, D_3 A_1 (\xi^m)^{-1} + D_4 B_1 + \left(D_5 B_2 + D_6 \varepsilon_r^c |_{\xi=\xi^m} + D_7 \varepsilon_\theta^c |_{\xi=\xi^m} \right) \xi^m \\
&+ \left(D_8 \frac{\partial \varepsilon_\theta^c}{\partial \xi} \Big|_{\xi=\xi^m} + \frac{\partial \varepsilon_r^c}{\partial \xi} \Big|_{\xi=\xi^m} \right) (\xi^m)^2.
\end{aligned}
\tag{29}
$$

The exact solution for Eq. (25) may be written as follows

$$U_g^m = \underbrace{K_1^m \exp(q_1^m \xi)}_{u_{g1}^m} + \underbrace{K_2^m \exp(q_2^m \xi)}_{u_{g2}^m},\tag{30}$$

$$q_1^m, q_2^m = \frac{-M_2^m \pm \sqrt{(M_2^m)^2 - 4 M_3^m P_1^m}}{2 M_1^m}.\tag{31}$$

The particular solution of the differential Eq. (25) may be obtained as follows

$$U_p^m = \xi^{q_1^m} u_1^m + \xi^{q_2^m} u_2^m,\tag{32}$$

where

$$u_1^m = -\int \frac{\xi^{q_2^m} R(\xi)|_{\xi=\xi^m}}{W(q_1^m, q_2^m)|_{\xi=\xi^m}}, \quad u_2^m = \int \frac{\xi^{q_1^m} R(\xi)|_{\xi=\xi^m}}{W(q_1^m, q_2^m)|_{\xi=\xi^m}},\tag{33}$$

where $R(\xi)$ is the expression on the right hand side of Eq. (25) and $W(\xi)$ is defined as:

$$W(q_1^m, q_2^m) = \begin{vmatrix} u_{g1}^m & u_{g2}^m \\ (u_{g1}^m)' & (u_{g2}^m)' \end{vmatrix}.\tag{34}$$

Combining Eqs. (31)–(34) one can obtain the particular solution as:

$$
\begin{aligned}
u_p^m = &\, \frac{D_3 \xi}{(q_2^m - 1)(q_1^m - 1)} A_1^m + \frac{D_4 \xi^3}{(q_2^m - 3)(q_1^m - 3)} B_1^m \\
&+ \frac{D_5 \xi^3}{(q_2^m - 3)(q_1^m - 3)} B_2^m + \frac{D_6 \xi^3}{(q_2^m - 4)(q_1^m - 4)} \varepsilon_r^c |_{\xi=\xi^m} \\
&+ \frac{D_7 \xi^3}{(q_2^m - 4)(q_1^m - 4)} \varepsilon_\theta^c |_{\xi=\xi^m} + \frac{\xi^4}{(q_2^m - 4)(q_1^m - 4)} \frac{\partial \varepsilon_r^c}{\partial \xi} \Big|_{\xi=\xi^m} \\
&+ \frac{D_8 \xi^4}{(q_2^m - 4)(q_1^m - 4)} \frac{\partial \varepsilon_\theta^c}{\partial \xi} \Big|_{\xi=\xi^m}.
\end{aligned}
\tag{35}
$$

Hence, the complete solution for U^m in terms of the non-dimensional radial coordinate is written as:

$$U^m = u_g^m + u_p^m, \quad \xi^m - \frac{h^m}{2} \leq \xi \leq \xi^m + \frac{h^m}{2}, \tag{36}$$

where h^m is the thickness of mth division, K_1^m and K_2^m are unknown constants for mth division. Substituting the displacement from Eq. (36) into Eq. (23), the radial and circumferential stresses are obtained as follows

$$\sigma_r = P_1^m \frac{\partial^2 \varepsilon_\theta^c}{\partial \xi^2}\bigg|_{\xi=\xi^m} + P_2^m \frac{\partial^2 \varepsilon_r^c}{\partial \xi^2}\bigg|_{\xi=\xi^m} + P_3^m \frac{\partial \varepsilon_\theta^c}{\partial \xi}\bigg|_{\xi=\xi^m} + P_4^m \frac{\partial \varepsilon_r^c}{\partial \xi}\bigg|_{\xi=\xi^m}$$
$$+ P_5^m \varepsilon_\theta^c\big|_{\xi=\xi^m} + P_6^m \varepsilon_r^c\big|_{\xi=\xi^m} + P_7^m K_2^m + P_8^m K_1^m + P_9^m A_1^m$$
$$+ P_{10}^m B_2^m + P_{11}^m B_1^m, \tag{37}$$

$$\sigma_\theta = P_{12}^m \frac{\partial^2 \varepsilon_\theta^c}{\partial \xi^2}\bigg|_{\xi=\xi^m} + P_{13}^m \frac{\partial^2 \varepsilon_r^c}{\partial \xi^2}\bigg|_{\xi=\xi^m} + P_{14}^m \frac{\partial \varepsilon_\theta^c}{\partial \xi}\bigg|_{\xi=\xi^m} + P_{15}^m \frac{\partial \varepsilon_r^c}{\partial \xi}\bigg|_{\xi=\xi^m}$$
$$+ P_{16}^m \varepsilon_\theta^c\big|_{\xi=\xi^m} + P_{17}^m \varepsilon_r^c\big|_{\xi=\xi^m} + P_{18}^m K_1^m + P_{19}^m K_2^m + P_{20}^m A_1^m$$
$$+ P_{21}^m B_1^m + P_{22}^m B_2^m, \tag{38}$$

where $P_i^m (i = 1, ...22)$ are expressed in Appendix B

Also, the electric potential can be obtained by integrating the combination of Eqs. (21) and (22) as follows

$$\Phi = \int \left(-\frac{A_1^m}{\xi^2} + E_1 \left(\frac{\partial U^m}{\partial \xi} - \alpha_r T^m(\xi) - \varepsilon_r^c\big|_{\xi=\xi^m} \right) \right.$$
$$\left. + 2E_2 \left(\frac{U^m}{\xi} - \alpha_\theta T^m(\xi) - \varepsilon_\theta^c\big|_{\xi=\xi^m} \right) \right) d\xi. \tag{39}$$

5.2. Boundary conditions

5.2.1. Continuity conditions

The unknowns K_1^m, K_2^m, B_1^m, B_2^m, A_1^m and A_2^m (the constant of integral in Eq. (39)) are determined by applying the necessary boundary conditions between two adjacent sub-domains. For this purpose, the continuity of radial displacement, radial stress and electric potential are imposed at the interfaces of the adjacent sub-domains. These continuity conditions at the interfaces are:

$$U^m\big|_{\xi=\xi^m + \frac{h^m}{2}} = U^{m+1}\big|_{\xi=\xi^{m+1} - \frac{h^{m+1}}{2}},$$
$$\frac{dU^m}{d\xi}\bigg|_{\xi=\xi^m + \frac{h^m}{2}} = \frac{dU^{m+1}}{d\xi}\bigg|_{\xi=\xi^{m+1} - \frac{h^{m+1}}{2}},$$
$$\sigma_r^m\big|_{\xi=\xi^m + \frac{h^m}{2}} = \sigma_r^{m+1}\big|_{\xi=\xi^{m+1} - \frac{h^{m+1}}{2}},$$
$$\Phi^m\big|_{\xi=\xi^m + \frac{h^m}{2}} = \Phi^{m+1}\big|_{\xi=\xi^{m+1} - \frac{h^{m+1}}{2}}, \tag{40}$$
$$T_\xi^m\big|_{\xi=\xi^m + \frac{h^m}{2}} = T_\xi^m\big|_{\xi=\xi^{m+1} + \frac{h^{m+1}}{2}},$$
$$\frac{\partial T_\xi^m}{\partial \xi}\bigg|_{\xi=\xi^m + \frac{h^m}{2}} = \frac{\partial T_\xi^m}{\partial \xi}\bigg|_{\xi=\xi^{m+1} + \frac{h^{m+1}}{2}},$$

5.2.2. Global boundary conditions

In this section, the appropriate electrical and mechanical boundary conditions are examined.

- Case 1: Mechanical boundary condition (the converse piezoelectric effect)

In case 1, the piezoelectric hollow sphere is subjected to an internal uniform pressure and zero electric potential difference. In this case, the sphere acts as an actuator.

$$\text{case 1}: \sigma_r(1) = -1, \quad \sigma_r(\eta) = 0, \quad \Phi(1) = 0, \quad \Phi(\eta) = 0, \tag{41}$$

- Case 2: Electrical boundary condition (the direct piezoelectric effect)

In case 2, free mechanical boundary conditions on both internal and external surfaces are imposed. However, in this case a uniform electrical potential difference is prescribed. In this case, the sphere acts as a sensor.

$$\text{case 2}: \sigma_r(1) = 0, \quad \sigma_r(\eta) = 0, \quad \Phi(1) = 1, \quad \Phi(\eta) = 0, \tag{42}$$

The continuity conditions (Eq. (40)) together with the global boundary conditions (Eqs. (41) and (42)) yield a set of linear algebraic equations in terms of K_1^m, K_2^m, A_1^m, A_2^m, B_1^m and B_2^m. Solving the resultant linear algebraic equations, the unknown coefficients are calculated. Then the displacement components, the stresses and the electric potential are determined in each radial sub-domain. Increasing the number of divisions improves the accuracy of the results. A brief flowchart of these procedures is shown in Fig. 3.

5.3. Time-dependent electro-thermo-elastic creep behavior of sphere

To obtain time-dependent stresses and electric potential, the creep strains in Eqs. (37)–(39) must be considered. Creep strain
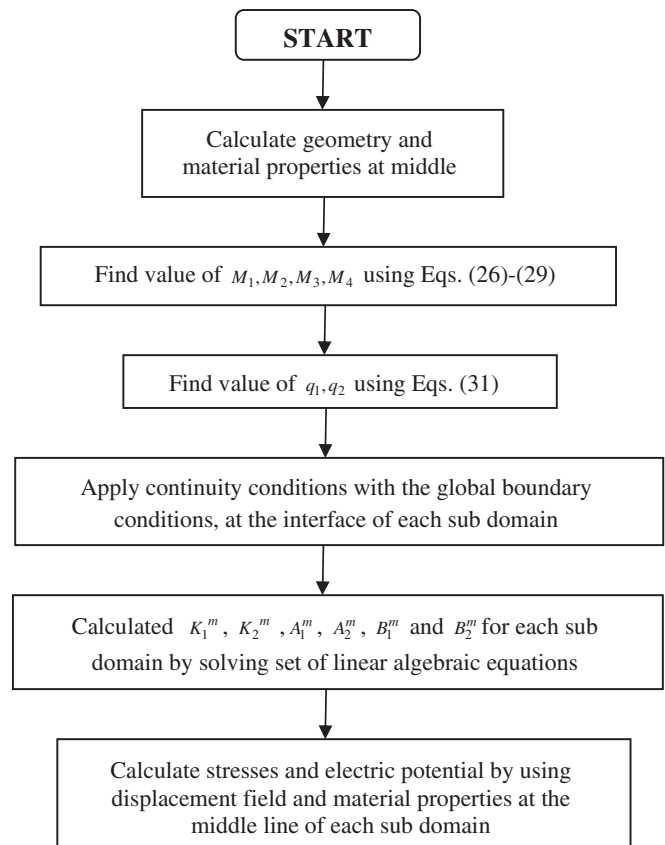

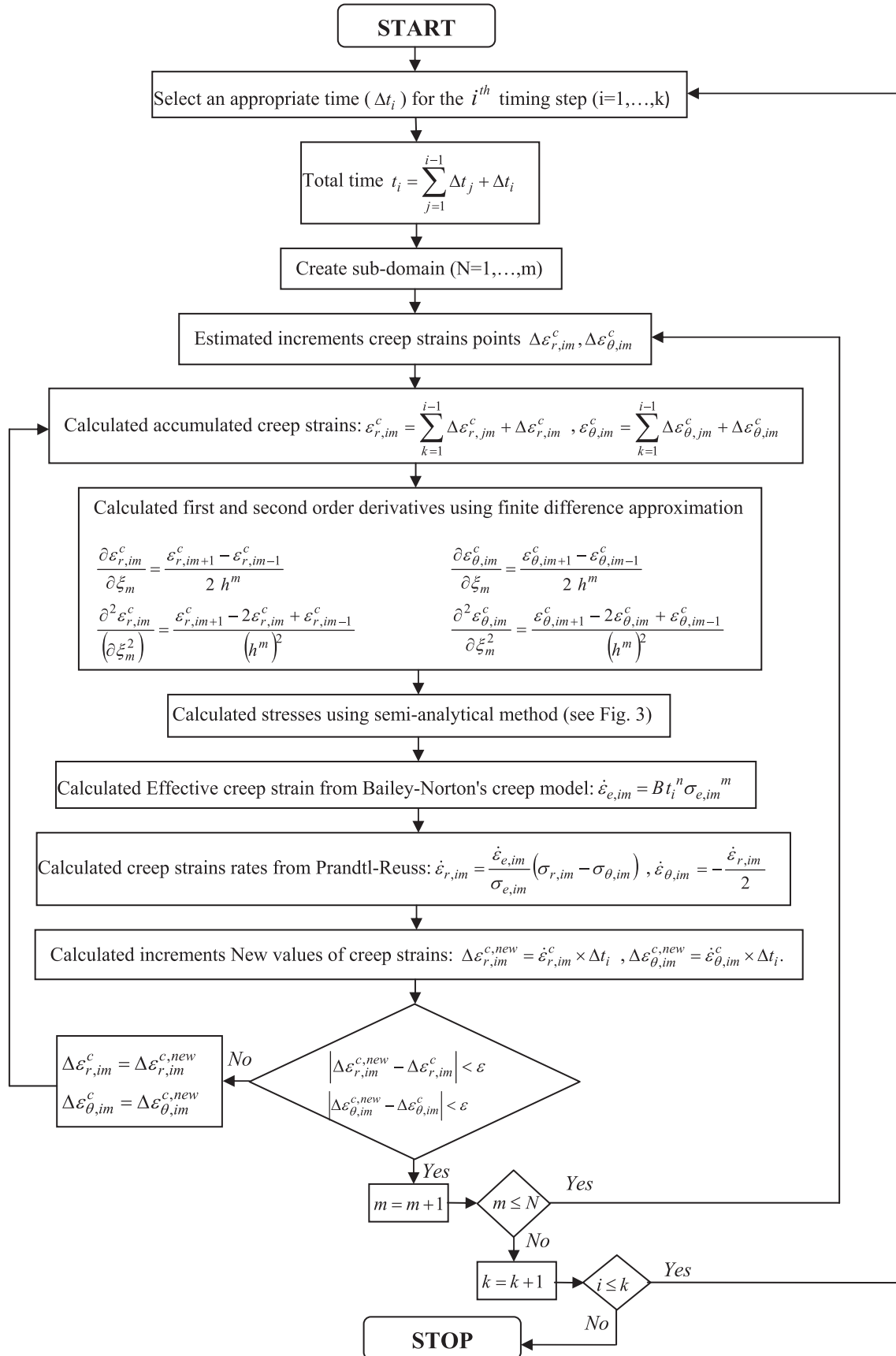**Fig. 3.** The flowchart of the semi-analytical method for a hollow sphere.

Fig. 4. The flowchart of the method of successive approximation (Mendelson) for a hollow sphere.
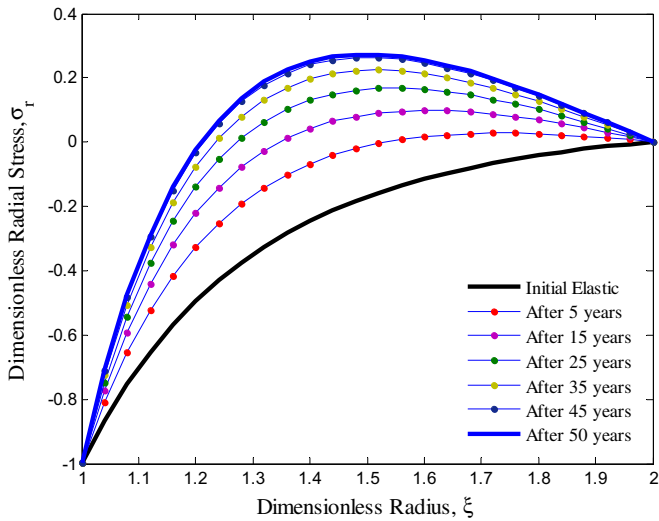
Fig. 5. The effect of time-dependent creep on the radial stress for mechanical boundary condition.

rates are related to the material uniaxial creep constitutive model and the current stress tensor by the well known Prandtl–Reuss relation. In this case Prandtl–Reuss relation is written as (Mendelson, 1968)

$$\dot{\varepsilon}_r = \frac{\dot{\varepsilon}_e}{\sigma_e}[\sigma_r - \sigma_\theta],$$

$$\dot{\varepsilon}_\theta = \dot{\varepsilon}_\zeta = -\frac{\dot{\varepsilon}_r}{2}. \qquad (43)$$

The Von Mises's effective stress for spherical symmetry is written as:

$$\sigma_e = \frac{1}{\sqrt{2}}\sqrt{(\sigma_\theta - \sigma_r)^2 + (\sigma_\theta - \sigma_\zeta)^2 + (\sigma_\zeta - \sigma_r)^2} = |\sigma_r - \sigma_\theta|. \qquad (44)$$

To obtain histories of stresses and deformation as well as electric potential, a numerical procedure on the basis of the method of successive approximation has been tailored.
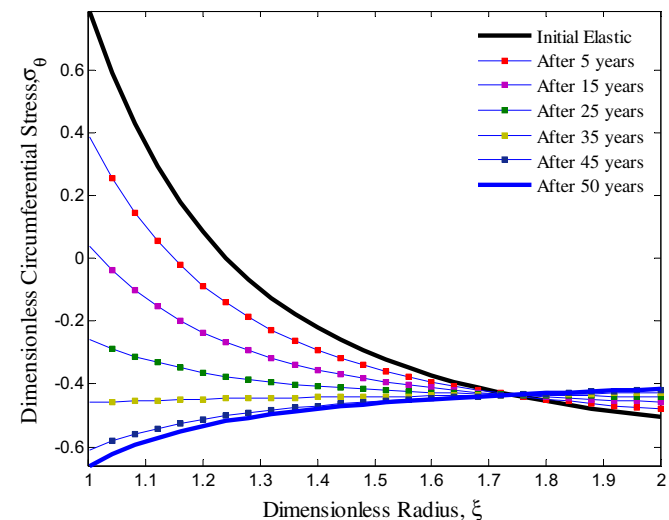

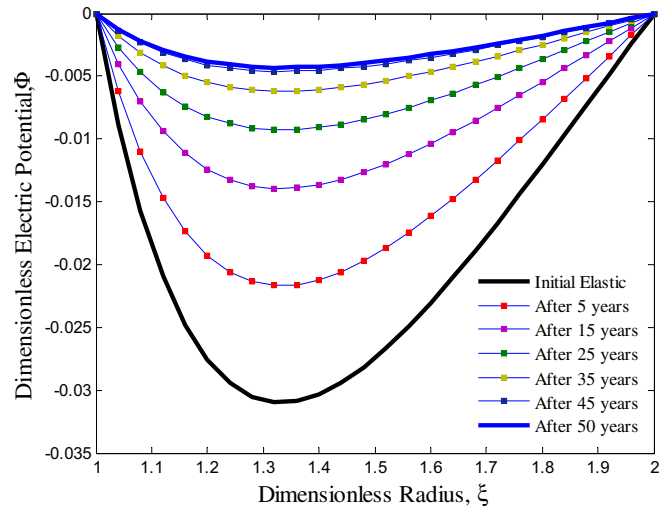**Fig. 6.** The effect of time-dependent creep on the circumferential stress for mechanical boundary condition.

Fig. 7. The effect of time-dependent creep on the electric potential for mechanical boundary condition.

5.4. Numerical procedure to obtain history of stresses, deformation and electric potential

We have employed Mendelson's method of successive elastic solution to obtain histories of stresses, electric potential and displacement as follows:

It was shown that creep strains and their derivatives are involved in non-homogenous part of differential Eq. (25). Immediately after loading, the creep strains are zero and the solution is an elasticity problem. To solve differential Eq. (25) for long time after loading, method of successive elastic solution is used. Step by step procedure is explained in Fig. 4.

6. Numerical results and discussion

Using the numerical procedure outlined in Section 5.4, the effects of time-dependent on electro-thermo-mechanical creep could be studied from Figs. 5–12, in which the histories of dimensionless radial and circumferential stresses, electric potential
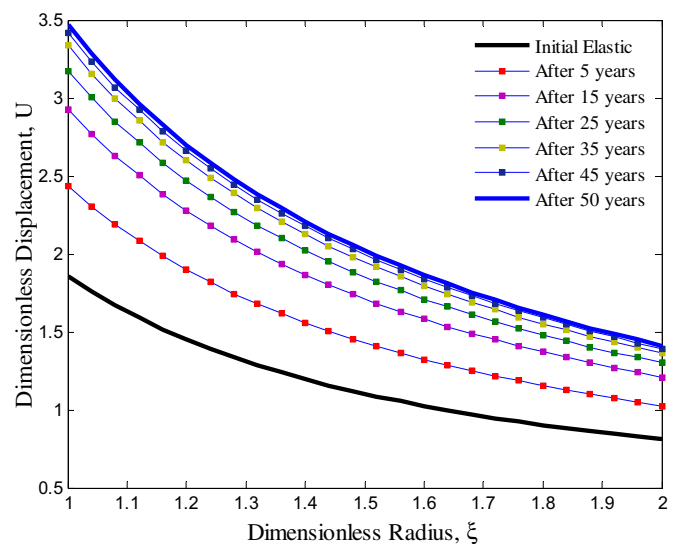

Fig. 8. The effect of time-dependent creep on the radial displacement for mechanical boundary condition.
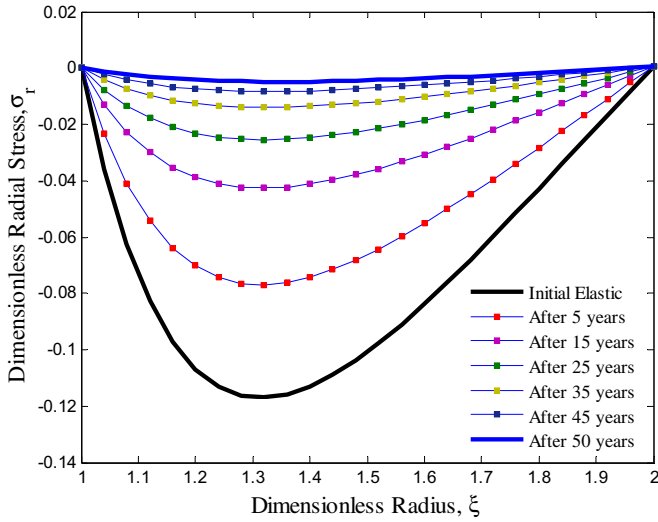
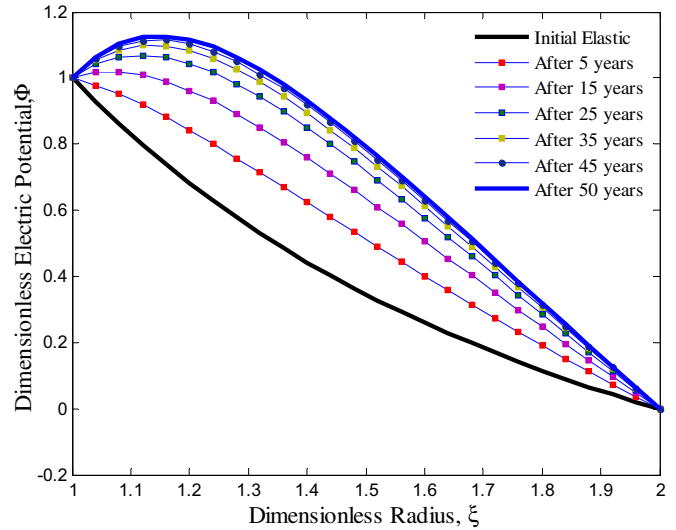**Fig. 9.** The effect of time-dependent creep on the radial stress for electrical boundary condition.

Fig. 11. The effect of time-dependent creep on the electric potential for electrical boundary condition.

and displacement versus dimensionless radius are illustrated in Figs. 5–8, respectively, for mechanical boundary condition and in Figs. 9–12 for electrical boundary condition.

The following general observations might be made from the above plots:

- Radial stresses and electric potential are constant with respect to time at the interior and exterior surfaces of the sphere, satisfying the constant mechanical and electrical boundary conditions.
- Radial stress, electric potential and radial displacement are increasing through-thickness with time at a decreasing rate so that there is a saturation condition beyond which not much change occurs.
- The history of the electric potential is fairly similar to that of the radial stress as far as the rate change is concerned. That is because the electric potential histories are induced by the

compressive radial stress histories during creep deformation of the sphere. This is expected from the piezoelectric characteristic point of view.

- The change in the rate of radial and circumferential stresses, electric potential and displacement, without commenting on the magnitude, become less significant after 25, begin to converge after 45, and reaches steady state after 50 years.

As for specific points, the following observations may be made:

- In mechanical boundary condition, which describes the converse piezoelectric effect and use in actuators, the effect of time-dependent creep causes to change radial stresses from compressive to tensile after 15 years. Hence, the actuators are not usable after 15 years and it must consider for actuators applications in modern technologies. It is argued that the actuators due to the layered structure, are mechanically fragile
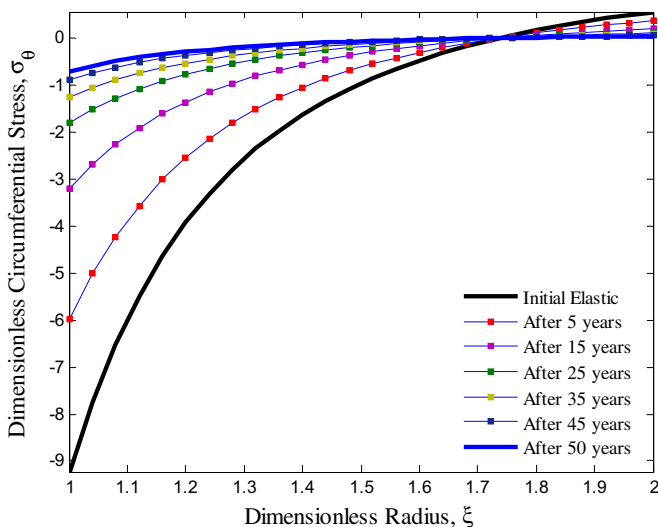

Fig. 10. The effect of time-dependent creep on the circumferential stress for electrical boundary condition.
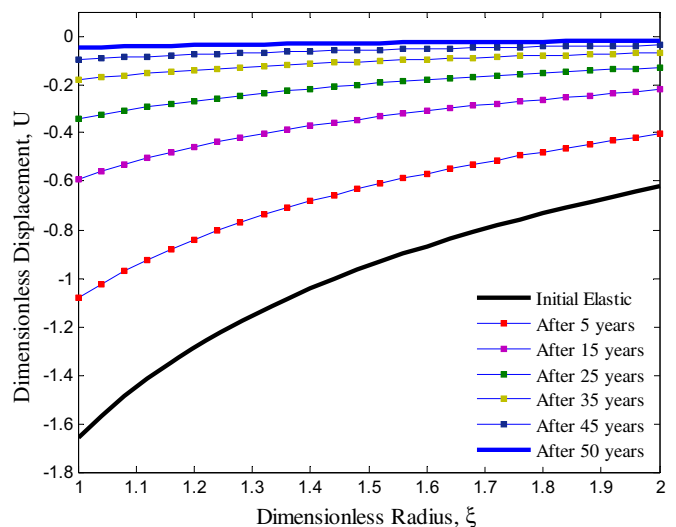

Fig. 12. The effect of time-dependent creep on the radial displacement for electrical boundary condition.

and as every piezoelectric ceramic, they are extremely sensitive to tensile loads.
- In electrical boundary condition, which describes the direct piezoelectric effect and use in sensors, the radial stresses are compressive during the life of the sphere. This state is suitable, because the sensors can be used for long time.
- For mechanical boundary condition, maximum change of radial stresses occurs in the 1.25–1.35 range of ξ, while for electrical boundary condition, minimum change of it occurs in the 1.25–1.35 range of ξ.
- A distinguished fixed (skeletal) point at which the stress does not change with time is observed for the circumferential stresses corresponding to ξ of 1.7–1.8. An attraction of the skeletal point concept is that it enables the stress state generated in a notch throat to be identified without a detailed knowledge of the creep properties of a material being available. It is noted that, Schulte (1960) was the first to observe this behavior and used it to predict the creep deformation.
- As far as the effect of time-dependent creep on circumferential stress is concerned, it decreases with time at the interior surface and increases with time at the exterior with decrease rates (maximum has occurred at the inner surface) for mechanical boundary condition, while for electrical boundary condition, it increases at the interior surface and decreases at the exterior surface with decrease rates (maximum has occurred at the outer surface).
- Maximum u occurs at the interior surface and it decreases smoothly towards the exterior for mechanical boundary condition, while for electrical boundary condition, Minimum u occurs at the interior surface and it increases smoothly towards the exterior.

7. Conclusions

In this research, for the first time, time-dependent creep behavior of a hollow radially polarized piezoelectric sphere subjected to electro-thermo-mechanical loading has been investigated using a semi-analytical numerical method, according to Mendelson's procedure.

For both mechanical and electrical boundary conditions which used in actuators and sensors, respectively, the effect of time-dependent creep on stresses, electric potentials and displacements are studied and presented graphically. Creep behavior of these is fairly similar as changes in the rates for these become less significant after 25, begin to converge after 45, and reaches steady state after 50 years of operation. Numerical analysis shows that in mechanical boundary condition, the effect of time-dependent creep causes to change radial stresses from compressive to tensile after 15 years. Hence, the actuators are not usable after 15 years and it must consider for actuators applications in modern technologies. The study also indicates that the radial stresses are compressive during the life of the sphere for electrical boundary condition. This state is suitable for sensors, because these can be used for long time. Also, a distinguished fixed (skeletal) point is observed for the circumferential stresses corresponding to ξ of 1.7–1.8 which used to predict the creep deformation.

Appendix A

$$D_1 = 3$$

$$D_2 = \frac{4C_2 + 4E_1E_2 - 2 - 2C_3 - 4E_2^2}{C_1 + E_1^2}$$

$$D_3 = \frac{2E_2}{C_1 + E_1^2}$$

$$D_4 = \frac{(3E_1 - 2E_2)(2E_2\alpha_\theta + E_1\alpha_r) + 3(2C_2\alpha_\theta + C_1\alpha_r) + ((1 + C_3)\alpha_\theta + C_2\alpha_r)}{\left(C_1 + E_1^2\right)}$$

$$D_5 = \frac{(-4C_1\alpha_r - (4E_1 + E_2)(2E_2\alpha_\theta + E_1\alpha_r)) - (2E_1 - E_2) + (2(1 + C_3)\alpha_\theta + 2C_2\alpha_r)}{\left(C_1 + E_1^2\right)} \qquad \text{(A.1)}$$

$$D_6 = -\frac{3\left(C_1 + E_1^2\right) + 2E_1^2 - 2E_1E_2 - 2C_2}{C_1 + E_1^2}$$

$$D_7 = -\frac{6(C_2 + E_1E_2) - 4E_2^2 - 4E_1E_2 - 2C_3 - 2}{C_1 + E_1^2}$$

$$D_8 = -\frac{2(C_2 + E_1E_2)}{C_1 + E_1^2}$$

Appendix B

$$P_1^m = (C_1 + E_1^2)\left(\frac{\xi^4 D_8}{(q_2^m - 4)(q_1^m - 4)}\right),$$

$$P_2^m = (C_1 + E_1^2)\left(\frac{\xi^4}{(q_2^m - 4)(q_1^m - 4)}\right),$$

$$P_3^m = \left(\frac{(2C_2 + C_1 + 2E_1E_2 + 4E_1)D_8\xi^3}{(q_2^m - 4)(q_1^m - 4)} + \frac{(2C_1 + E_1)\xi^3 D_7}{(q_2^m - 3)(q_1^m - 3)}\right),$$

$$P_4^m = \left(\frac{(2C_2 + C_1 + 2E_1E_2 + 4E_1)\xi^3}{(q_2^m - 4)(q_1^m - 4)} + \frac{(2C_1 + E_1)\xi^3 D_6}{(q_2^m - 3)(q_1^m - 3)}\right),$$

$$P_5^m = \left(\frac{(2C_2 + 3C_1 + 2E_1E_2 + 3E_1^2)D_7\xi^2}{(q_2^m - 3)(q_1^m - 3)} - 2(E_1E_2 + C_2)\right),$$

$$P_6^m = \left(\frac{(2C_2 + 3C_1 + 2E_1E_2 + 3E_1^2)D_6\xi^2}{(q_2^m - 3)(q_1^m - 3)} - (E_1^2 + C_1)\right),$$

$$P_7^m = \left((2C_2 + C_1q_2 + 2E_1E_2 + E_1^2q_2)\xi^{q_2 - 1}\right),$$

$$P_8^m = \left((2C_2 + C_1q_1 + 2E_1E_2 + E_1^2q_1)\xi^{q_1 - 1}\right),$$

$$P_9^m = \left(\frac{(2C_2 + 2E_1E_2 + (E_1^2 + C_1))D_3}{(q_2^m - 1)(q_1^m - 1)} - 2E_1\xi^{-2}\right),$$

$$P_{10}^m = \left(\frac{(2C_2 + 2E_1E_2 + 3(E_1^2 + C_1))D_5\xi^2}{(q_2^m - 3)(q_1^m - 3)} - (2C_2\alpha_\theta + C_1\alpha_r)\right),$$

$$P_{11}^m = \left(\frac{(2C_2 + 2E_1E_2 + 3(E_1^2 + C_1))D_4\xi^2}{(q_2^m - 3)(q_1^m - 3)} + (2(C_2 + E_2)\alpha_\theta + (C_1 + E_1)\alpha_r)\xi^{-1}\right),$$

$$P_{12}^m = (C_2 + E_1E_2)\left(\frac{\xi^4}{(q_2^m - 4)(q_1^m - 4)}\right),$$

$$P_{13}^m = (C_1 + E_1^2)\left(\frac{\xi^4}{(q_2^m - 4)(q_1^m - 4)}\right),$$

$$P_{14}^m = \left(\frac{((1 + C_3) + C_2 + 4E_1E_2 + E_2^2)D_8\xi^3}{(q_2^m - 4)(q_1^m - 4)} + \frac{(4C_2 + E_1)\xi^3 D_7}{(q_2^m - 3)(q_1^m - 3)}\right),$$

$$P_{15}^m = \left(\frac{((1 + C_3) + C_2 + 4E_1E_2 + E_2^2)D_8\xi^3}{(q_2^m - 4)(q_1^m - 4)} + \frac{(4C_2 + E_1)\xi^3 D_7}{(q_2^m - 3)(q_1^m - 3)}\right),$$

$$P_{16}^m = \left(\frac{((1 + C_3) + 3C_2 + 3E_1E_2 + 2E_2^2)D_7\xi^2}{(q_2^m - 3)(q_1^m - 3)} - (2E_2^2 + (1 + C_3))\right),$$

$$P_{17}^m = \left(\frac{((1 + C_3) + 3C_2 + 3E_1E_2 + 2E_2^2)D_6\xi^2}{(q_2^m - 3)(q_1^m - 3)} - (E_1E_2 + C_2)\right),$$

$$P_{18}^m = \left(((1 + C_3) + C_2q_1 + E_1E_2q_1 + 2E_2^2)\xi^{q_1 - 1}\right),$$

$$P_{19}^m = \left(((1 + C_3) + 2E_2^2 + E_1E_2q_2 + C_2q_2)\xi^{q_2 - 1}\right),$$

$$P_{20}^m = \left(\frac{((1 + C_3) + 2E_1E_2 + 2E_2^2 + (E_1E_2 + C_2))D_3\xi}{(q_2^m - 1)(q_1^m - 1)} - (E_2)\xi^{-2}\right),$$

$$P_{21}^m = \left(\frac{((1 + C_3) + 3C_2 + 2E_2^2 + 3E_1E_2)D_4\xi^2}{(q_2^m - 3)(q_1^m - 3)}\right),$$

$$P_{22}^m = \left(\frac{((1 + C_3) + 2E_2^2 + 3(E_1E_2 + C_2))D_5\xi^2}{(q_2^m - 3)(q_1^m - 3)} - ((1 + C_3 + 2E_2^2)\alpha_\theta + (C_2 + E_1E_2)\alpha_r)\right).$$

(B.1)

References

Babaei, M.H., Chen, Z.T., 2008. Analytical solution for the electromechanical behavior of a rotating functionally graded piezoelectric hollow shaft. Arch. Appl. Mech. 78, 489—500.

Bayat, M., Saleem, M., Sahari, B.B., Hamouda, A.M.S., Mahdi, E., 2009. Mechanical and thermal stresses in a functionally graded rotating disk with variable thickness due to radially symmetry loads. Int. J. Pres. Ves. Pip. 86, 357—372.

Chen, J.J., Tu, Sh.T., Xuan, F.Zh., Wang, Zh.D., 2006. Creep analysis for a functionally graded cylinder subjected to internal and external pressure. J. Strain. Anal. 42, 69—77.

Dai, H.L., Fu, Y.M., 2006. Electromagnetotransient stress and perturbation of magnetic field vector in transversely isotropic piezoelectric solid spheres. Mate. Sci. Eng. B 129, 86—92.

Dai, H.L., Wang, X., 2005. Thermo-electro-elastic transient response. Int. J. Solids Struct. 42, 1151—1171.

Fungn, Y.C., 1965. Foundations of Solid Mechanics. Prentice-Hall, New York.

Ghorbanpour Arani, A., Golabi, S., Saadatfar, M., 2006. Stress and electric potential fields in piezoelectric smart spheres. J. Mech. Sci. Technol. 20, 1920—1933.

Ghorbanpour Arani, A., Kolahchi, R., Mosallaie Barzoki, A.A., 2011. Effect of material in-homogeneity on electro-thermo-mechanical behaviors of functionally graded piezoelectric rotating shaft. Appl. Math. Model. 35, 2771—2789.

Ghorbanpour Arani, A., Salari, M., Khademizadeh, H., Arefmanesh, A., 2010. Magnetothermoelastic stress and perturbation of magnetic field vector in a functionally graded hollow sphere. Arch. Appl. Mech. 80, 189—200.

Hamed, E., 2012. Bending and creep buckling response of viscoelastic functionally graded beam-columns. Compos. Struct. 94, 3043—3051.

Jabbaria, M., Sohrabpourb, S., Eslami, M.R., 2002. Mechanical and thermal stresses in a functionally graded hollow cylinder due to radially symmetric loads. Int. J. Pres. Ves. Pip. 79, 493—497.

Jalili, N., 2010. Piezoelectric-based Vibration Control from Macro to Micro/Nano Scale Systems. Springer Science, New York.

Khoshgoftar, M.J., Ghorbanpour Arani, A., Arefi, M., 2009. Thermoelastic analysis of a thick walled cylinder made of functionally graded piezoelectric material. Smart. Mater. Struct. 18 (115007), 8.

Kordkheili, S.A.H., Naghdabadi, R., 2007. Thermoelastic analysis of a functionally graded rotating disk. Compos. Struct. 79, 508—516.

Loghman, A., Aleayoubb, S.M.A., Hasani Sadi, M., 2012. Time-dependent magneto-thermoelastic creep modeling of FGM spheres using method of successive elastic solution. Appl. Math. Model. 36, 836—845.

Loghman, A., Ghorbanpour Arani, A., Aleayoub, S.M.A., 2011a. Time-dependent creep stress redistribution analysis of thick-walled functionally graded spheres. Mech. Time Dep. Mat. 15, 353—365.

Loghman, A., Ghorbanpour, A., Amir, S., Vajedi, A., 2010. Magnetothermoelastic creep analysis of functionally graded spheres. Int. J. Pres. Ves. Pip. 87, 389—395.

Loghman, A., Ghorbanpour Arani, A., Shajari, A.R., Amir, S., 2011b. Time-dependent thermoelastic creep analysis of rotating disk made of Al—SiC composite. Arch. Appl. Mech. 81, 1853—1864.

Loghman, A., Shokouhi, N., 2009. Creep damage evaluation of thick-walled spheres using a long-term creep constitutive model. J. Mech. Sci. Technol. 23, 2577—2582.

Loghman, A., Wahab, M.A., 1996. Creep damage simulation of thick-walled tubes using the theta projection concept. Int. J. Pres. Ves. Pip. 67, 105—111.

Mendelson, A., 1968. Plasticity: Theory and Applications. Macmillan Company, New York.

Penny, R.K., Marriott, D.L., 1995. Design for Creep. CHAPMAN & HALL, London.

Saadatfar, M., Razavi, A.S., 2009. Piezoelectric hollow cylinder with thermal gradient. J. Mech. Sci. Technol. 23, 45—53.

Salehi-Khojin, A., Jalili, N., 2008. A comprehensive model for load transfer in nanotube reinforced piezoelectric polymeric composites subjected to electro-thermo-mechanical loadings. Compos. B 39, 986—998.

Schulte, C.A., 1960. Predicting creep deflections of plastic beams. Proc. ASTM 60, 895—904.

Spathis, G., Kontou, E., 2012. Creep failure time prediction of polymers and polymer composites. Compos. Sci. Tech. 72, 959—964.

Tejeet, S., Gupta, V.K., 2011. Effect of anisotropy on steady state creep in functionally graded cylinder. Compos. Struct. 93, 747—758.

Tiersten, H.F., 1969. Linear Piezoelectric Plate Vibrations. Plenum Press, New York.

Wang, H.M., Xu, Z.X., 2010. Effect of material inhomogeneity on electromechanical behaviors of functionally graded piezoelectric spherical structures. Comput. Mater. Sci. 48, 440—445.

Xuan, F.Z., Chen, J.J., Wang, Z., Tu, S.T., 2009. Time-dependent deformation and fracture of multi-material systems at high temperature. Int. J. Pres. Ves. Pip. 86, 604—615.

Yang, Y.Y., 2000. Time-dependent stress analysis in functionally graded materials. Int. J. Solids Struct. 37, 7593—7608.

Yazdani, H., O'Dowd, N.P., 2012. Study of creep relaxation under combined mechanical and residual stresses. Eng. Frac. Mech. 93, 132—152.

You, L.H., Ou, H., Zheng, Z.Y., 2007. Creep deformations and stresses in thick-walled cylindrical vessels of functionally graded materials subjected to internal pressure. Compos. Struct. 78, 285—291.

Zhou, D., Kamlah, M., 2006. Room-temperature creep of soft PZT under static electrical and compressive stress loading. Acta Mater. 54, 1389—1396.

Zolochevsky, A., Martynenko, A., Kühhorn, A., 2012. Structural benchmark creep and creep damage testing for finite element analysis with material tension—compression asymmetry and symmetry. Comput. Struct. 100, 27—38.